Rapid Communications

Unexpected electric-field-induced antiferroelectric liquid crystal phase in the SmC_α^* temperature range and the discrete flexoelectric effect

Yoichi Takanishi,[1,*] Atsuo Iida,[2] Neelam Yadav,[3] A. D. L. Chandani Perera,[3,4] Atsuo Fukuda,[3]
Mikhail A. Osipov,[5,6] and Jagdish K. Vij [3,†]

[1]*Department of Physics, Kyoto University, Kyoto 606-8502, Japan*
[2]*Photon Factory, Institute of Materials Structure Science, High Energy Accelerator Research Organization, Ibaraki 305-0801, Japan*
[3]*Department of Electronic and Electrical Engineering, Trinity College Dublin, The University of Dublin, Dublin 2, Ireland*
[4]*Department of Chemistry, University of Peradeniya, Peradeniya 20400, Sri Lanka*
[5]*Department of Mathematics and Statistics, University of Strathclyde, Glasgow G1 1XH, United Kingdom*
[6]*Topchiev Institute of Petrochemical Synthesis, Russian Academy of Sciences, Moscow 119991, Russia*

The unique nanometer-sized helical structure in SmC_α^* may sometimes evolve continuously to the micrometer-sized one in SmC^*; conceivably ferroelectric SmC_α^* is to be unwound by an applied electric field. By drawing electric-field-induced birefringence contours in the field-temperature phase diagram and by studying the superlattice structure of the field-induced subphase with resonant x-ray scattering, we established that an applied field unexpectedly stabilizes the well-known antiferroelectric four-layer biaxial subphase as well as the other prototypal ferrielectric three-layer one in the SmC_α^* temperature range; the effective long-range interlayer interaction due to the discrete flexoelectric effect actually plays an important role in stabilizing not only the biaxial subphases but also the optically uniaxial SmC_α^* subphase, contrary to the notion that the competition between the direct interactions of the nearest-neighbor layers and those of the next-nearest-neighbor layers should be required for the nanometer-sized helical structure.

The discovery of the phenomena of ferroelectricity and antiferroelectricity in liquid crystals has been reported in [1,2]. The phenomenon involves frustration of synclinic SmC^* and anticlinic SmC_A^* at the phase transition point. The clinicity frustration together with long-range interlayer interaction (LRILI) produces several biaxial smectic subphases, such as ferrielectric 1/3 with the three-layer unit cell (FAA), antiferroelectric 1/2 with the four-layer unit cell (FAFA), etc. [3–5]. Here we designate the subphase as the ratio $q_T = [F]/([F] + [A])$, where $[F]$ and $[A]$ are the numbers of ferroelectric and antiferroelectric orderings in the unit cell. Recently, the definite existence of subphases 1/4 and 2/5 with eight- and ten-layer unit cells, respectively, was vindicated by studying electric-field-induced birefringence (EFIB) and microbeam resonant x-ray scattering (μRXS) [6,7]. This indicates the importance of the *effective* LRILI based on the seminal "discrete flexoelectric effect" [8], as any *direct* LRILI to produce the ten-layer ordered superlattice structure is hard to consider in smectics with no long-range positional order. Notice also that the effective LRILI naturally predicts the nonflat, highly distorted nanometer-sized helical structure of the biaxial subphases experimentally observed [9,10]. In solid state physics such extended structures are repeatedly encountered in various systems. Actually, the sequential emergence of subphases used to be understood by using the Ising and/or X-Y models in magnetism in connection with the Devil's staircase [11–13].

It should be noted, however, that such treatments could not explain the nanometer-sized helical structure.

In addition to these chiral tilted smectic phases, SmC_A^* and SmC^*, their orthogonal counterpart SmA also participates in the frustration and produces the optically uniaxial smectic subphase SmC_α^* with the nanometer-sized helical structure of incommensurate pitch, which can sometimes evolve continuously to the micrometer-sized one in SmC^* on cooling [14,15]; conceivably ferroelectric SmC_α^* is to be unwound by an applied electric field [16]. In fact, Yamashita's group analyzed the unwinding process from a standpoint of discrete soliton excitation and showed its staircase character with ferrielectriclike states, although they did not take any effects of LRILI into account [17,18]. In this Rapid Communication we report that an applied field unexpectedly stabilizes antiferroelectric four-layer 1/2 as well as ferrielectric three-layer 1/3 in the SmC_α^* temperature range; these stabilizations indicate that the same effective LRILI plays an important role in the formation of SmC_α^* itself, although its nanometer-sized helical structure is often incorrectly considered to be produced by the competition between the direct interactions of the nearest-neighbor layers and those of the next-nearest-neighbor layers [19]. In other words, it is the discrete flexoelectric effect that produces a very strong chiral interaction [20].

Samples investigated here were pure MHPOCBC and a binary mixture of MHPOCBC (80 wt %) with AS657 (20 wt %). The chemical structures of these compounds are given in Fig. 2 of Ref. [7]. Experimental studies were made by the complementary methods: EFIB in homeotropically aligned cells to obtain the field-temperature (E-T) phase diagram with birefringence contours and μRXS in homogeneously

---

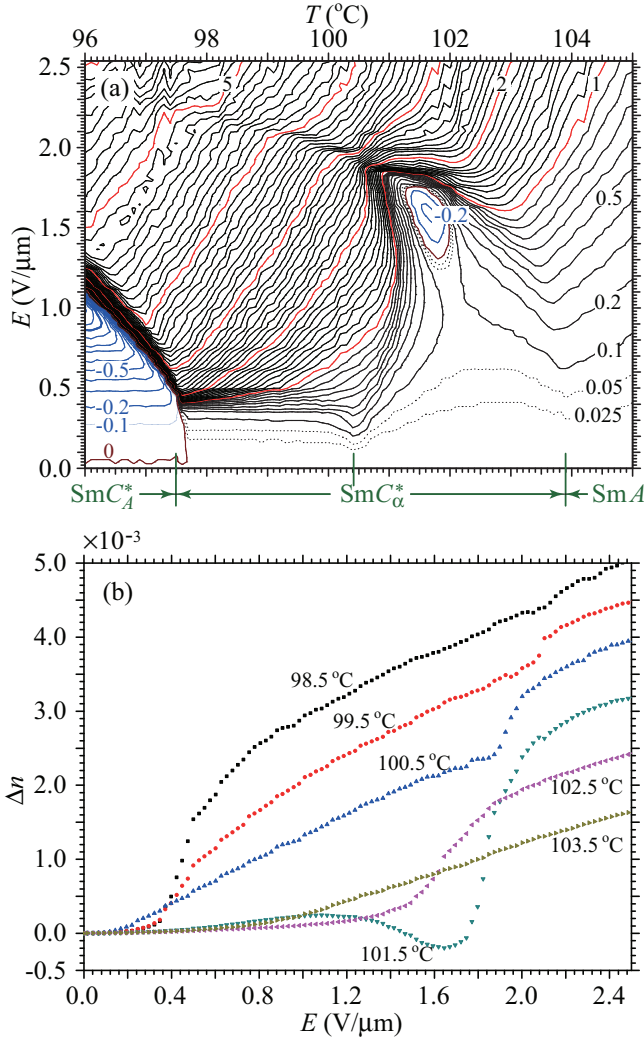*Corresponding author: ytakanis@scphys.kyoto-u.ac.jp
†Corresponding author: jvij@tcd.ie

FIG. 1. The EFIB result of pure MHPOCBC: (a) The E-T phase diagram with the contours of constant birefringence and (b) the Δn-E plots.
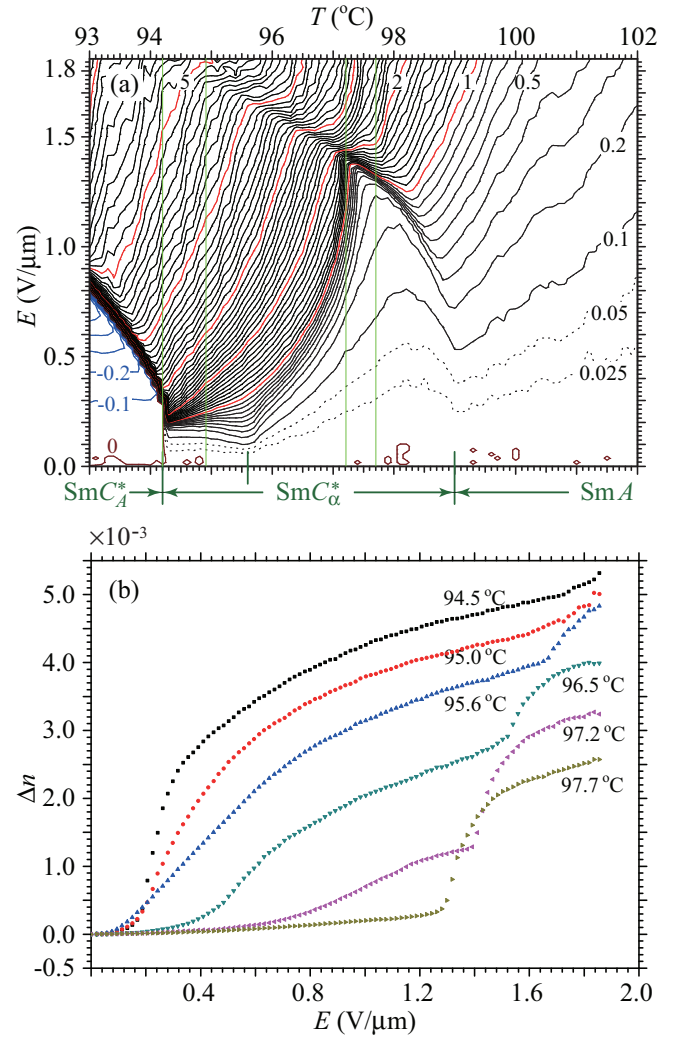

FIG. 2. The EFIB result of the mixture of MHPOCBC (80 wt %) with AS657 (20 wt %): (a) The E-T phase diagram with the contours of constant birefringence and (b) the Δn-E plots.

aligned (smectic layers almost perpendicular to substrate plates) planar cells to determine the superlattice structure of the field-induced subphases. We refer to the previous papers [6,7] for the experimental details; in particular, we followed the conventions that the electric field was applied along the y axis and that EFIB was defined as $\Delta n = n_x - n_y$ as in the previous papers.

The EFIB result of pure MHPOCBC shown in Fig. 1(a) apparently behaves quite differently in the low- and high-temperature regions of SmC_α^*. Below about 100 °C, the densely populated contour lines almost parallel to the T axis indicate the field-induced phase transition of SmC_α^* to ferrielectric 1/3 as pointed out previously [21]. In fact, Δn stays almost zero at fields lower than 0.2 V/μm, increases rather steeply at around 0.4 V/μm, gradually becomes larger up to about 2 V/μm, and then increases steeply again, as can be seen in Fig. 1(b); the steep increases at around 0.4 and 2 V/μm must represent the field-induced phase transition to 1/3 and unwound SmC^*, respectively. Since the tilt angle in SmC_α^* is less than about 7°, it becomes larger with increasing field even after transition to unwound SmC^* due

to the electroclinic effect. In the high-temperature region, on the other hand, we can see some negative closed contours unexpectedly in Fig. 1(a). In fact, as clearly seen in Fig. 1(b), Δn becomes negative at around 1.6 V/μm for 101.5 °C. In between low- and high-temperature regions there appears to exist the intermediate one around 100.4 °C.

Note that antiferroelectric 1/2 and SmC_A^* are known to show negative closed contours as the applied field unwinds the macroscopic helix and makes the averaged tilt plane approximately parallel to the field [22–24]. Recalling this characteristic feature prompts us to consider that the negative closed contours in Fig. 1(a) suggest the emergence of a field-induced antiferroelectric 1/2 subphase. In order to confirm that its superlattice structure comprises four-layer unit cells using μRXS techniques, we needed to add some Se-containing compound in our accessible facilities. Actually we prepared the MHPOCBC-AS657 mixture and measured EFIB. The mixture shows the EFIB results given in Fig. 2, which do not change much from those of pure MH-POCBC in Fig. 1. We can see the low- and high-temperature ranges of SmC_α^* in Fig. 2(a) as well as the characteristic
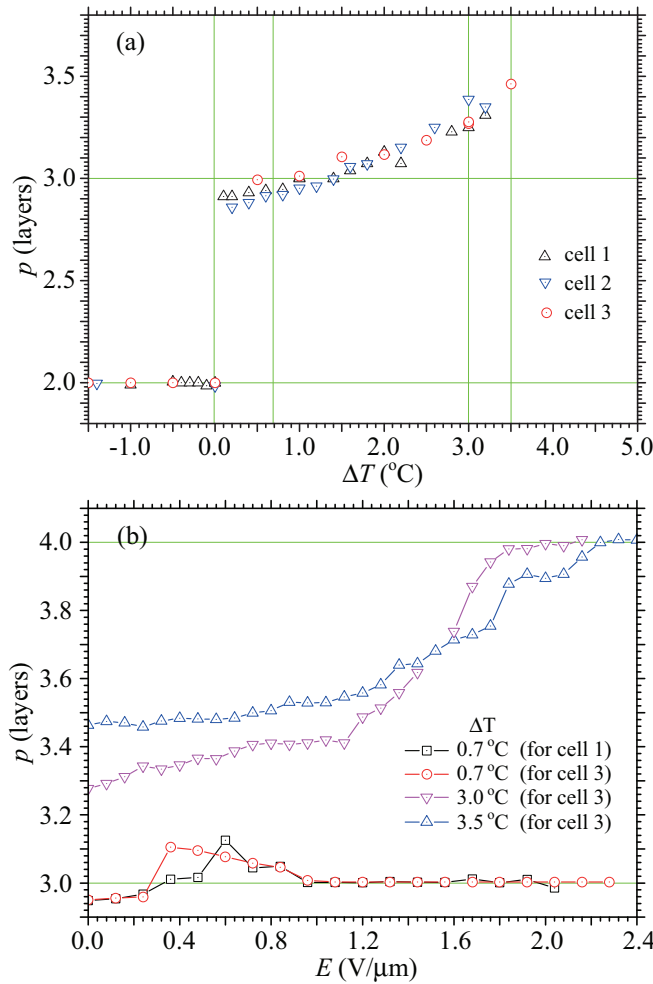
FIG. 3. The μRXS result of the mixture of MHPOCBC (80 wt %) with AS657 (20 wt %): (a) The temperature variation of the SmC_α^* nanometer-sized helical pitch and (b) the field dependence of superlattice periodicities at $\Delta T = 0.7$, 3.0, and 3.5 °C. Here ΔT is the relative temperature measured from the transition point between SmC_A^* and SmC_α^*; $\Delta T = 0$ and the above three ΔT's correspond to 94.2, 94.9, 97.2, and 97.7 °C in Fig. 2(a), shown by thin green vertical lines.

behavior of Δn vs E curves in the low- (94.5 and 95.0 °C), intermediate- (95.6 and 96.5 °C), and high- (97.2 and 97.7 °C) temperature regions in Fig. 2(b).

Figure 3 summarizes the μRXS peak positions as functions of (a) temperature and (b) applied field in the mixture. The temperature variation shows that the short pitch of the SmC_α^* nanometer-sized helical structure elongates gradually on heating, but that it is smaller than three layers up to about 1.3 °C above the SmC_A^*-SmC_α^* transition temperature. This short-pitch range of less than three layers corresponds to the low-temperature range where Δn stays almost zero at fields lower than 0.1 V/μm and increases rather steeply at around 0.2 V/μm; hence it is natural to conjecture that an applied increasing field elongates the SmC_α^* short pitch up to three layers and then changes SmC_α^* into the field-induced subphase 1/3. It is stably realized in a reasonably wide field range as seen in Fig. 3(b) and the distortion angle of 1/3 decreases with increasing field, for Δn becomes larger in

Fig. 2(b). As shown in Fig. 3, furthermore, we can see that the SmC_α^* short pitch becomes longer than three layers with rising temperature but does not seem to exceed four layers; likewise, an applied increasing field elongates the SmC_α^* short pitch up to four layers and stabilizes a field-induced subphase with a four-layer unit cell at least in the high-temperature region reasonably separated from the transition point to SmA. Furthermore, because of the similarity between Fig. 1 and Fig. 2, we can conclude that this field-induced subphase with a four-layer unit cell is antiferroelectric 1/2.

Now we try to understand theoretically the field-induced emergence of ferrielectric three-layer 1/3 and antiferroelectric four-layer 1/2 in the SmC_α^* temperature range. We need to consider the three-phase frustration among SmC_A^*, SmC^*, and SmA and the resulting degeneracy lifting by LRILI at zero field. There are two theoretical approaches to describe the sequential emergence of biaxial subphases: One is the phenomenological Landau model reported by Dolganov *et al.* [25–27] and the other is the partial molecular model with the effective LRILI due to the discrete flexoelectric effect [8,28]. The nanometer-sized helical structure of uniaxial SmC_α^* is often incorrectly considered to be produced by the competition between the direct interactions of the nearest-neighbor layers and those of the next-nearest-neighbor layers on the premise that a very strong chiral interaction could not be identified [19]; it is questionable whether any direct interactions between nonadjacent smectic layers are practically strong enough, though. Actually the effective LRILI based on the discrete flexoelectric effect takes into account the direct interactions between adjacent layers only, and these successfully explained the highly distorted nanometer-sized helical structure of the biaxial subphases; this LRILI can also apply to understanding the nanometer-sized helical structure of SmC_α^* [20,29,30], although any systematic detailed study has not been made yet. Since the aforementioned experimental facts indicate that the *same* LRILI must play an important role in the emergence of not only the biaxial subphases but also uniaxial SmC_α^*, we use the effective LRILI due to the discrete flexoelectric effect [8,20,28] in the following.

The short-range interlayer interaction (SRILI) is extended to treat the three-phase frustration by taking into account the temperature dependence of the tilt angle Θ as detailed in Ref. [31]. In order to reduce the number of parameters to describe the phase diagram, we regard Θ itself as an effective temperature [32], so that the phase transition from SmA occurs at $\Theta = 0$ with the transition temperature T_0; hereafter the whole interaction energies are divided by $k_B T_0$ and made dimensionless. For simplicity, the molecular biaxiality is not taken into account and the nematic and smectic order is considered perfect; then the free energy for SRILI is a function of three scalar variables, $(\mathbf{n}_1 \cdot \mathbf{n}_2)$, $(\mathbf{n}_1 \cdot \mathbf{e})$, and $(\mathbf{n}_2 \cdot \mathbf{e})$, where $\mathbf{n}_1$ and $\mathbf{n}_2$ are directors in adjacent layers and $\mathbf{e}$ is the smectic layer normal. In the approximation of the spatially uniform tilt angle, we have $(\mathbf{n}_1 \cdot \mathbf{e}) = (\mathbf{n}_2 \cdot \mathbf{e}) = \cos\Theta$ and $(\mathbf{n}_1 \cdot \mathbf{n}_2) = \cos^2\Theta + \sin^2\Theta \cos\varphi_{12}$ where $\varphi_{12} = \varphi_2 - \varphi_1$ is the difference between the corresponding azimuthal angles that specify the orientation of the tilt planes. The free energy pertaining to synclinic SmC^* is expanded in spherical invariants preserving the lowest order nonpolar terms, i.e., quadratic in $\mathbf{n}_1$ and $\mathbf{n}_2$. Since conventional

dispersion and steric interactions between mesogenic molecules generally promote SmC^*, only two terms in the expansion with coefficients $V_1 = v_1^{\parallel}/k_B T_0$ and $V_3 = v_3^{\parallel}/k_B T_0$ are effective; here $V_{\text{eff}} = -(3V_1 + V_3) > 0$ characterizes the SmC^* stability and $V_{1,\text{eff}} = V_1/V_{\text{eff}}$ is the Maier-Saupe type effective interaction parameter.

Anticlinic SmC_A^* is stabilized by interlayer orientational correlations between transverse molecular dipoles located in the flexible chains, which are also written as nonpolar terms up to quadratic in $\mathbf{n}_1$ and $\mathbf{n}_2$ [31]; hence the SmC_A^* stability is specified by the dimensionless dipole moment $\mu = d_{\perp}/\{(2k_B T_0)^{1/2}(R_{12}^{\parallel})^{3/2}\}$, where $d_{\perp}$ and $R_{12}^{\parallel}$ are the transverse dipoles and the distance between them of neighboring molecules in adjacent layers. In this way the free energy for SRILI can be written in the dimensionless form with two parameters $r = \mu^4/V_{\text{eff}}$, the relative stability ratio between SmC_A^* and SmC^*, and $V_{1,\text{eff}}$ as

$$- (1 - r\,\sec^6 \Theta)\cos\varphi_{i,i+1}$$
$$- \tan^2 \Theta\left(-\tfrac{3}{2}V_{1,\text{eff}} + \tfrac{1}{4}r\,\sec^6 \Theta\right)\cos^2 \varphi_{i,i+1}. \quad (1)$$

The total free energy at zero field in the dimensionless form $\mathcal{F}_0$ is obtained by adding to Eq. (1) the LRILI terms given in Eq. (62) of Ref. [8] for any t-layer biaxial subphase or the corresponding term given in Eq. (A.7) of Ref. [20] for uniaxial SmC_{α}^*; the strength ratio of LRILI to SRILI is now written as $\mathcal{R} = \chi c_f c_p/(k_B T_0 V_{\text{eff}})$ instead of $\chi c_f c_p/B$ to allow for appropriate nondimensionalization. The total free energy contains only six dimensionless parameters; in addition to the already explicitly mentioned four, (i) r, (ii) Θ, (iii) $\mathcal{R}$, and (iv) $V_{1,\text{eff}} < 0$, there are two parameters originally introduced by Emelyanenko and Osipov [8]: (v) g the molecular positional correlation in adjacent layers and (vi) c_f/c_p the ratio of the flexoelectric and piezoelectric coefficients. By using the first two parameters as the abscissa and ordinate of the phase diagram, we can draw the r-Θ phase diagram, checking which subphase obtained above, biaxial or uniaxial, has actually the lower total free energy. Notice that $\mathcal{R}$ has the same sign as $c_f c_p$ and that their sign determines the handedness of the nanometer-sized helical structure; $c_f c_p < 0$ corresponds to the right-handed helix and vice versa.

The previous investigations suggest $g \approx 0.2$ and $c_f/c_p \approx -1$ [8,28]. Trial calculations were made rather systematically for the remaining parameter value combinations of $\mathcal{R} = -0.02$ to -0.2 and $V_{1,\text{eff}} = -1$ to -50. We drew plenty of r-Θ phase diagrams and chose Fig. 4 almost uniquely that can successfully reproduce the experimental results summarized in Figs. 1–3. The tilt angle Θ represents the effective temperature and the subphase emerging sequence of a particular compound or mixture is given by a $r = \text{const}$ line. The solid line curve running from an upper right (0,1) point to a lower left (40,0.2) point in Fig. 4(a) represents the boundary between exactly anticlinic SmC_A^* and exactly synclinic SmC^* for $\mathcal{R} = 0$; all the biaxial subphases are degenerate into the solid line curve as no LRILI is taken into account. When it comes to $\mathcal{R} \neq 0$, degeneracy is lifted and biaxial subphases emerge in the "slug-shaped" finite area around the solid line curve as illustrated in Fig. 4(a). When the line crosses the slug-shaped biaxial subphase area in its body part [see Fig. 4(a-1)], we can
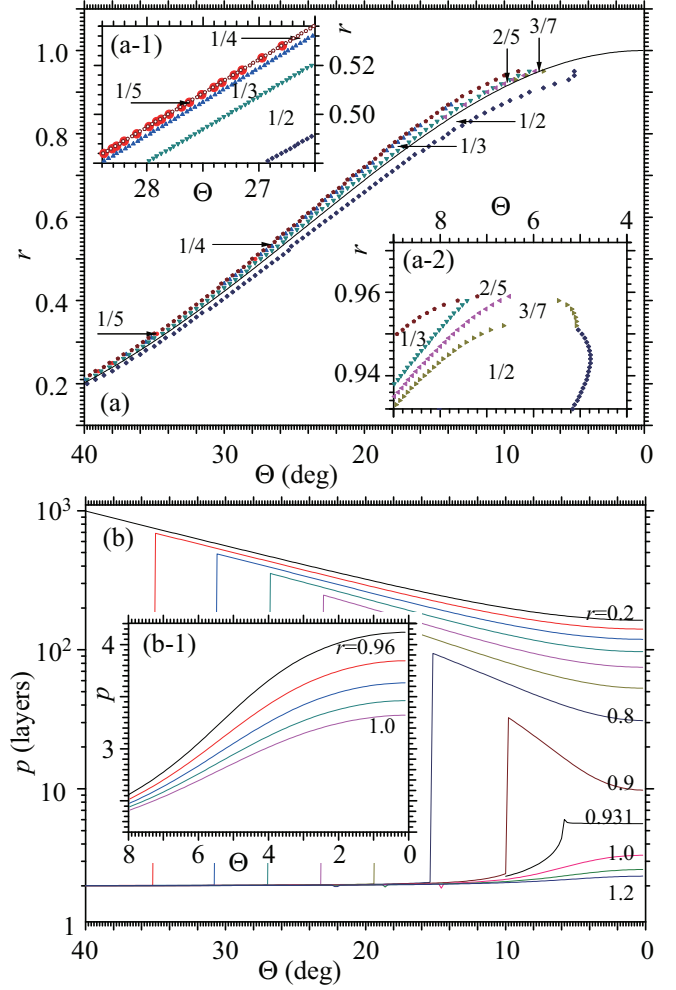

FIG. 4. Summaries of calculated results for parameter values of $c_f/c_p = -1$, $g = 0.2$, $\mathcal{R} = -0.02$, $V_{1,\text{eff}} = -2$: (a) The r-Θ phase diagram and (b) the SmC_{α}^* (SmC^* and SmC_A^*) helical pitch vs Θ for $r = 0.2$–1.2 at a step of 0.1. Insets (a-1) and (a-2), and (b-1) are expanded plots in the specified Θ-r and Θ-p spaces, respectively.

see the standard phase sequence:

$$\text{Sm}C_A^* - \tfrac{1}{5} - \tfrac{1}{4} - \mathbf{\tfrac{1}{3}} - \tfrac{2}{5} - \tfrac{3}{7} - \mathbf{\tfrac{1}{2}} - \text{Sm}C^*,$$

although 1/5, 1/4, 2/5, and 3/7 may or may not emerge depending on the parameter values. In the upper head part of the slug-shaped biaxial subphase area [for detail, see Fig. 4(a-2)], on the other hand, the phase emerging sequence is quite irregular; e.g., any of 1/4, 1/3, 2/5, and 3/7 can singly emerge between SmC_A^* and SmC^* (SmC_{α}^*) for appropriately chosen parameter values.

Outside the biaxial subphase area, both SmC_A^* and SmC^*, otherwise purely anticlinic and synclinic since the ordinary weak chiral interaction is not taken into account, now acquire the helical structure; in other words, we can say that SmC_{α}^* appears when the pitch becomes nanometer sized as explained below in detail. The helical pitch in the unit of the number of smectic layers can be obtained from $\varphi_{i,i+1}$ that minimizes $\mathcal{F}_0$ for uniaxial SmC_{α}^*. Figure 4(b) illustrates some calculated results for parameters used to obtain Fig. 4(a). Notice that helical pitches are drawn even in the area of the Θ-r space

where SmC$_\alpha^*$ does not have the lowest $\mathcal{F}_0$, i.e., even in the inside of the biaxial subphase area. For a small $r(= 0.2$, e.g.) and a large $\Theta(= 40°$, e.g.), SmC* has a micrometer-sized pitch (of $p = 10^3$); the pitch may become nanometer sized and SmC* is suitably called SmC$_\alpha^*$ for a large r and a small Θ. In this approximate calculation the change between SmC* and SmC$_\alpha^*$ is always continuous; experimentally both continuous and discontinuous changes were observed [14,15]. When the pitch becomes close to $p = 2$ for a large Θ, the phase can be regarded as SmC$_A^*$ with a macroscopic pitch of $1/\{(1/p) - 0.5\}$, which may be of micrometer size as that of SmC* but the handedness is just opposite [33,34]. For $r \geqslant 0.96$ it does not cross the biaxial subphase area and SmC$_A^*$ continuously changes into SmC$_\alpha^*$; experimentally no continuous change has been observed between them.

As Θ approaches zero, the helical pitch of SmC$_\alpha^*$ becomes longer for $r > 0.931$ and vice versa. In particular, as illustrated in the inset of Fig. 4(b) the SmC$_\alpha^*$ helical pitch in terms of the number of smectic layers increases from approximately 2.8 to 3.8 layers with decreasing Θ from 6.5 to 0° at around $r = 0.97$, which can almost reproduce the experimentally observed one given in Fig. 3(a). Now we try to see whether any of the biaxial three- and four-layer subphases actually has the free energy less than that of unwound SmC* before an applied field attains the complete unwinding of SmC$_\alpha^*$; notice that there are two four-layer subphases, antiferroelectric 1/2 (FAFA) and ferrielectric 1/2 (FFAA), and only one three-layer subphase, ferrielectric 1/3 (FAA). The free energy under an applied electric field $\mathcal{F}$ for these subphases as well as unwound SmC* can be obtained by adding the effective electric field term as given in Eq. (17) of Ref. [24] to $\mathcal{F}_0$ at zero field. For the sake of simplicity, no electroclinic effect is taken into account, i.e., Θ is considered to be independent of E; then the coefficient term containing E as a whole can be treated as a dimensionless effective field $\mathcal{E}$ in actual calculations. In the case of ferrielectric subphases and unwound SmC* it is straightforward to obtain the effective free energy $\mathcal{F}$ under an applied field $\mathcal{E}$ following the procedures described in Sec. IV A of Ref. [24]. In the case of antiferroelectric 1/2, on the other hand, we can adopt Eq. (25) of Ref. [24] and obtain $\mathcal{F}$ in likewise. Figure 5 summarizes the calculated results for the same parameter values used in Fig. 4. For $r = 0.97$ and $\Theta = 6°$, SmC$_\alpha^*$ has lower $\mathcal{F}_0$ than any others, 1/3, antiferroelectric 1/2, ferrielectric 1/2, and unwound SmC* at $\mathcal{E} = 0$, but 1/3 comes to have $\mathcal{F}$ lower than $\mathcal{F}_0$ of SmC$_\alpha^*$ at $\mathcal{E} = 0.02$ and stays lowest up to $\mathcal{E} = 0.08$, and then $\mathcal{F}$ of unwound SmC* becomes lowest. When $\Theta = 4°$ for $r = 0.97$, on the other hand, antiferroelectric 1/2 comes to have the lowest $\mathcal{F}$ among other biaxial phases, 1/3, ferrielectric 1/2, and unwound SmC*, in a reasonably wide range of up to $\mathcal{E} = 0.05$. Since an applied field could not reduce $\mathcal{F}$ of antiferroelectric 1/2 sufficiently, however, $\mathcal{F}_0$ of SmC$_\alpha^*$ stays lower than $\mathcal{F}$ of antiferroelectric 1/2 in the whole $\mathcal{E}$ range.

In this way the present simplified model preliminarily explains that an applied field stabilizes the well-known antiferroelectric four-layer 1/2 biaxial subphase as well as the other prototypal one, ferrielectric three-layer 1/3, in the temperature range of optically uniaxial SmC$_\alpha^*$. At the same time, the frustration among SmC$_A^*$, SmC*, and SmA
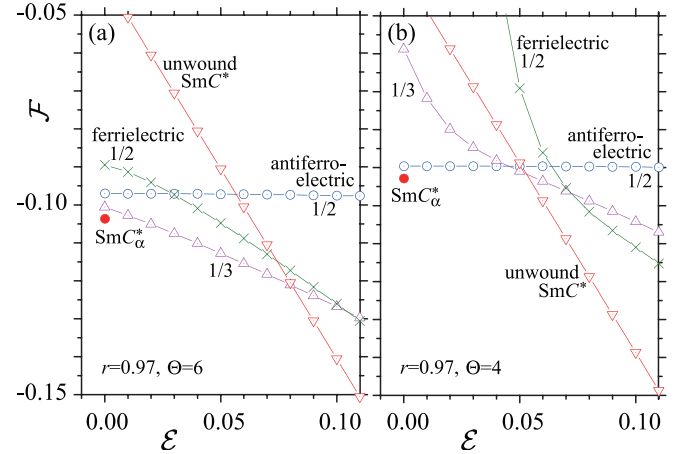

FIG. 5. The calculated free energy $\mathcal{F}$ vs an applied effective field $\mathcal{E}$ for unwound SmC*, antiferroelectric 1/2, 1/3, and ferrielectric 1/2 at (a) $\Theta = 6$ and (b) 4°; the free energy $\mathcal{F}_0$ for SmC$_\alpha^*$ is also shown. The parameters used are the same as in Fig. 4 and $r = 0.97$.

and the degeneracy lifting due to the effective LRILI based on the discrete flexoelectric effect well describes the overall picture of the resulting not only biaxial but also uniaxial subphases. Notice that, in the context of the present model, $\mathcal{F}$ of antiferroelectric four-layer 1/2 is higher than that of SmC$_\alpha^*$ even in the presence of the electric field. Since the difference is relatively small, however, a number of weak factors may reverse the difference. In particular, there is a well-known dielectric contribution to $\mathcal{F}$ which has not been taken into account because it is quadratic in the field. This contribution is negative and is approximately proportional to the birefringence of the smectic phase in the plane of the layers. Thus this contribution reduces $\mathcal{F}$ of the antiferroelectric four-layer 1/2 biaxial subphase. In contrast, it practically does not affect $\mathcal{F}$ of SmC$_\alpha^*$ because it is uniaxial. Notice also that at small tilt angles the birefringence is quadratic in the tilt angle and hence the dielectric contribution is rather small. On the other hand, the term which distinguishes between ferro- and antiferroelectric order is also quadratic in the tilt angle. Therefore the dielectric contribution may in principle drive $\mathcal{F}$ of antiferroelectric four-layer 1/2 below that of SmC$_\alpha^*$ and thus explain the experimentally observed stabilization of antiferroelectric four-layer 1/2 in the external electric field. Regarding the discontinuous change between SmC$_A^*$ and SmC$_\alpha^*$ experimentally observed, Sandhya et al. [35] pointed out the importance of the higher order terms in the (aforementioned) expansion of the free energy pertaining to synclinic SmC*; it is expanded in spherical invariants preserving the lowest order nonpolar terms containing $\cos \varphi_{i,i+1}$ and $\cos^2 \varphi_{i,i+1}$ as in Eq. (1). The expansion is a reasonable approximation near the minima at around $\varphi_{i,i+1} = 0°$ and 180°; since the change from SmC$_\alpha^*$ to SmC* or SmC$_A^*$ would occur far apart from these two minima, however, the higher order terms must play a crucial role. We suspect that this higher-order-term effect must also help to reduce $\mathcal{F}$ of the field-induced antiferroelectric four-layer 1/2 subphase efficiently.

[1] R. B. Meyer, L. Liebert, L. Strzelecki, and P. Keller, J. Phys. Lett. (France) **36**, L69 (1975).

[2] A. D. L. Chandani, E. Gorecka, Y. Ouchi, H. Takezoe, and A. Fukuda, Jpn. J. Appl. Phys. **28**, L1265 (1989).

[3] J. Prost and R. Bruinsma, Ferroelectrics **148**, 25 (1993).

[4] R. Bruinsma and J. Prost, J. Phys. (France) **4**, 1209 (1994).

[5] A. Fukuda, Y. Takanishi, T. Isozaki, K. Ishikawa, and H. Takezoe, J. Mater. Chem. **4**, 997 (1994).

[6] Z. Feng, A. D. L. Chandani Perera, A. Fukuda, J. K. Vij, K. Ishikawa, A. Iida, and Y. Takanishi, Phys. Rev. E **96**, 012701 (2017); A. D. L. Chandani, N. M. Shtykov, V. P. Panov, A. V. Emelyanenko, A. Fukuda, and J. K. Vij, *ibid.* **72**, 041705 (2005).

[7] A. D. L. Chandani Perera, A. Fukuda, J. K. Vij, and Y. Takanishi, Liq. Cryst. **44**, 1787 (2017).

[8] A. V. Emelyanenko and M. A. Osipov, Phys. Rev. E **68**, 051703 (2003).

[9] P. M. Johnson, D. A. Olson, S. Pankratz, T. Nguyen, J. Goodby, M. Hird, and C. C. Huang, Phys. Rev. Lett. **84**, 4870 (2000).

[10] L. S. Matkin, S. J. Watson, H. F. Gleeson, R. Pindak, J. Pitney, P. M. Johnson, C. C. Huang, P. Barois, A.-M. Levelut, G. Srajer, J. Pollmann, J. W. Goodby, and M. Hird, Phys. Rev. E **64**, 021705 (2001).

[11] P. Bak, Phys. Today **39**(12), 38 (1986).

[12] Y. Takanishi, K. Hiraoka, V. K. Agrawal, H. Takezoe, A. Fukuda, and M. Matsushita, Jpn. J. Appl. Phys., Part 1 **30**, 2023 (1991).

[13] T. Matsumoto, A. Fukuda, M. Johno, Y. Motoyama, T. Yui, S.-S. Seomun, and M. Yamashita, J. Mater. Chem. **9**, 2051 (1999).

[14] C. D. Cruz, J. C. Rouillon, J. P. Marcerou, N. Isaert, and H. T. Nguyen, Liq. Cryst. **28**, 125 (2001).

[15] A. Cady, D. A. Olson, X. F. Han, H. T. Nguyen, and C. C. Huang, Phys. Rev. E **65**, 030701(R) (2002).

[16] V. Bourny and H. Orihara, Phys. Rev. E **63**, 021703 (2001).

[17] M. Yamashita, *in Solitons in Liquid Crystals*, edited by L. Lam and J. Prost (Springer-Verlag, New York, 1992), Chap. 10, pp. 293–325.

[18] Y. Sakai, M. Torikai, and M. Yamashita, Mol. Cryst. Liq. Cryst. **516**, 81 (2010).

[19] D. A. Olson, S. Pankratz, P. M. Johnson, A. Cady, H. T. Nguyen, and C. C. Huang, Phys. Rev. E **63**, 061711 (2001).

[20] K. L. Sandhya, J. K. Vij, A. Fukuda, and A. V. Emelyanenko, Liq. Cryst. **36**, 1101 (2009).

[21] K. Hiraoka, Y. Takanishi, H. Takezoe, A. Fukuda, T. Isozaki, Y. Suzuki, and I. Kawamura, Jpn. J. Appl. Phys., Part 1 **31**, 3394 (1992).

[22] T. Qian and P. L. Taylor, Phys. Rev. E **60**, 2978 (1999).

[23] L. A. Parry-Jones and S. J. Elston, Appl. Phys. Lett. **79**, 2097 (2001).

[24] A. D. L. Chandani, A. Fukuda, J. K. Vij, Y. Takanishi, and A. Iida, Phys. Rev. E **93**, 042707 (2016).

[25] P. V. Dolganov and V. M. Zhilin, Phys. Rev. E **87**, 062505 (2013).

[26] P. V. Dolganov and E. I. Kats, Liq. Cryst. Rev. **1**, 127 (2014).

[27] P. V. Dolganov, Phys. Rev. E **98**, 032707 (2018).

[28] A. Fukuda, Mol. Cryst. Liq. Cryst. **610**, 1 (2015).

[29] N. M. Shtykov, A. D. L. Chandani, A. V. Emelyanenko, A. Fukuda, and J. K. Vij, Phys. Rev. E **71**, 021711 (2005).

[30] A. V. Emelyanenko, A. Fukuda, and J. K. Vij, Phys. Rev. E **74**, 011705 (2006).

[31] M. A. Osipov and A. Fukuda, Phys. Rev. E **62**, 3724 (2000).

[32] A. V. Emelyanenko and K. Ishikawa, Soft Matter **9**, 3497 (2013).

[33] V. Laux, N. Isaert, G. Joly, and H. T. Nguyen, Liq. Cryst. **26**, 361 (1999).

[34] J. P. F. Lagerwall, F. Giesselmann, and M. Osipov, Liq. Cryst. **33**, 625 (2006).

[35] K. L. Sandhya, A. D. L. Chandani, A. Fukuda, S. Kumar, and J. K. Vij, Phys. Rev. E **87**, 062506 (2013).

Correction: A minor error in text for the definition of *r* appearing in the paragraph before Eq. (1) has been fixed. Reference [13] contained a production error and has been fixed.